Journal of the European Ceramic Society **15** (1995) 573–579

0955-2219/95/$9.50

0955-2219(95)00018-6

Transmission Electron Microscopy of Intergranular Regions of Corroded Silicon Nitride

A. D. Stalios,[a] J. Luyten,[a] F. L. Riley[b]* & R. J. Fordham[c]

[a]Materials Department, SCK/VITO, B-2400 Mol, Belgium
[b]School of Materials, The University of Leeds, Leeds LS2 9JT, UK
[c]Materials Centre, JRC Petten, 1755 ZG Petten, The Netherlands

(Received 17 March 1994; revised version received 18 January 1995; accepted 26 January 1995)

Abstract

Two hot-pressed, dense, silicon nitride materials have been exposed to the flue gases of an aluminium smelting furnace heavily contaminated with Al, Ca and K-containing dust and vapours. Transmission electron microscopy (TEM) has been used to examine microstructural changes occurring in the silicon nitride at the interface between corroded and uncorroded material. Extensive diffusion of contaminant metal into the intergranular glass of the silicon nitride occurs, associated with physical and chemical changes in the intergranular regions, and a marked loss of mechanical strength.

1 Introduction

Silicon nitride ceramics are being considered for use as structural components in heat-exchangers in a range of industrial processes. One example is the aluminium remelting furnace where waste heat recovery would be expected to lead to significant energy savings. During the refining operation considerable amounts of a fluoride and chloride flux are added to the metal to form slags. The flue gases can thus contain high concentrations of salts, and silicate byproducts, and they are highly corrosive towards the non-oxide ceramics such as silicon carbide and silicon nitride. Most reported high temperature corrosion studies on silicon nitride have been carried out under closely defined and simplified laboratory conditions. A small number of studies have also been made involving the exposure of silicon carbide and silicon nitride materials to high temperature working industrial environments.[1–3] The work reported here was part of a study carried out to identify the major consequences of corrosive degradation of dense multiphase silicon nitride materials under severe industrial conditions.

Previous detailed studies on silicon nitride[4–8] have concentrated attention on the mechanism of surface oxidative corrosion with relatively thin (~20 μm) layers of corrodent oxide, or with continuous supplies of volatile corrodent at low vapour pressure. It has been shown that surface reactions, and phase equilibrium relationships, involving silicon dioxide and the oxide components of the corrosion film of the type:

$$M_aO_{b(s)} + SiO_{s(s)} = M_aSiO_{(2+b)(l)}$$

are of importance in controlling the rate of corrosion. Surface equilibria can also determine the extent of corrosion caused by a specific amount of corrodent oxide. Liquid silicates of composition not in thermodynamic equilibrium with silicon dioxide (SiO_2) are effectively solvents for SiO_2 and thus prevent the formation of potentially protective films on the silicon nitride surface. These laboratory studies have shown the importance of actual or incipient SiO_2 films at the silicon nitride–silicate film interface as oxygen transport barriers,[9] and therefore able to provide resistance against corrosion. The oxygen conductivity of pure SiO_2 in amorphous and crystalline form is low: silicate glasses and liquids are markedly more permeable towards oxygen.[10]

Detailed attention has not been paid to processes occurring in the silicon nitride beneath the surface oxide film during high temperature corrosion, and under conditions where the formation of a protective SiO_2 layer may be difficult. The microstructure of the silicon nitride is an important factor, and in particular the presence of the interconnecting siliceous intergranular glass. Intergranular cations are particularly important during oxidation in that they are able to diffuse from the intergranular phase to the surface oxide film to react to form silicates. The outwards diffusion of metal cation then becomes an important component of the rate controlling process.[11] However,

*To whom all correspondence should be addressed.

during high temperature oxidative corrosion under conditions where high concentrations of metal cations are deposited on the outer surface of the nitride, inwards diffusion of these cations into the intergranular glass will also occur. One consequence will be a change in composition of the glass, to one richer in contaminant metal oxide and of lower viscosity,[12] and resulting in the silicon nitride having lower high temperature strength and creep resistance. There exists also the possibility of internal oxidation through the rapid transport of oxygen to the silicon nitride grains through the more conductive intergranular glass or liquid. The implications for the long term structural stability and load-bearing capability of the component are thus considerable.

The object of the study reported here was to detect the existence of such inwards diffusion processes by examination of the intergranular regions of the silicon nitrides close to the surface corrosion product film, using transmission electron microscopy (TEM) on thinned foils. Two dense commercial grades of hot-pressed silicon nitrides were used for this study: one (designated SN1) had been densified using yttrium oxide (Y_2O_3); the other (SN2) had been formed using magnesium oxide (MgO). Both contained iron (the SN1 less than the SN2) which had been used possibly either as a silicon nitridation catalyst in the production of the silicon nitride powder, or as a densification aid.[13] The microstructure of the MgO-densified SN2 has already been discussed with regard to the function of iron during the hot-pressing densification stage.[14]

These materials were mounted in refractory concrete holders in an industrial continuous operation aluminium scrap remelting furnace, and exposed for extended times to the flue waste gases at temperatures in the region of 1050°C.

2 Experimental

The chemical compositions of the two commercial hot-pressed silicon nitrides (Feldmühle, Plochingen, Germany), expressed in terms of weight % of oxide constituent (or the equivalent), are given in Table 1.

Small test bars of material, of dimension 14 × 7 × 7 mm^3, were partly embedded in a block of refractory concrete and mounted in the wall of the flue gas duct of a standard large aluminium remelting furnace (Aluminium Foundries, R. Claeys, Lichtervelde, Belgium) fired by three natural gas burners. Two thermocouples were fixed to the concrete blocks with their tips close to the silicon nitride bars. The furnace was operated normally for times up to 1000 h during which time

Table 1. Silicon nitride composition/wt%

	SN1	SN2
Y_2O_3	9·0	0·005
MgO	0·005	1·2
Al_2O_3	0·12	0·20
Fe_2O_3	1·7	2·7
CaO	0·05	0·25
ZrO_2	0·01	0·01
[Si_3N_4	balance	balance]

the temperature fluctuated between 1000 and 1100°C with a mean of 1050°C. Flue gases were contaminated with chlorides and fluorides used as slag-forming fluxes in earlier furnace operating cycles. Exposed bars were removed, and sectioned for examination across the regions which had been fully in the flue gas flow. Scrapings of deposit from corroded surfaces were milled and analyzed by X-ray diffraction (XRD).

TEM examinations (JEOL 200CX equipped with a LaB_6 filament operating at 200 kV) were made of ion-beam thinned discs cut from as-received, and exposed, plates of material 7 × 14 × 0·5 mm^3. The more loosely adhering surface scale was carefully brushed away from each oxidised plate, and the silicon nitride mechanically ground from the unreacted side of the plate to give a maximum thickness of 150 μm. Discs 3 mm in diameter were drilled from the thinned plate and dimpled from both sides until the corrosion layer–bulk material interface was barely visible. Uncorroded materials were prepared in the standard way. Discs were then further ion-milled to perforation in a Gatan 600 dual ion mill using argon ions at 6 kV with a 15° incidence angle, and were finally coated with a 20 nm carbon film to prevent charging in the electron beam. The samples of corroded silicon nitride used for TEM examination were therefore planar sections approximately parallel to the corroded surface (rather than sections normal to the external surface) in the vicinity of the interface between uncorroded, and corroded, material.

The mechanical strengths in four-point bend (Instron Universal test equipment) of as-received and corroded materials were measured before and after exposure to flue gas, using a self-aligning fixture (span 40/20 mm) and a crosshead speed of 6 μm s^{-1}.

3 Results

3.1 The corrosion environment

Two typical random analysis of the flue gases during the course of normal corrosion tests are given in Table 2. These showed that while the tempera-

Table 2. Two examples of typical flue gas exposure conditions

Mean temperature/°C	1020	1090
Gas velocity/m s^{-1}	2·8	3·0
O_2/%	0·1–0·8	1·3–14·2
H_2O/%	19·7	5·4
CO_2/%	9·9–11·5	3·2–12·0
CO/ppm*	19 800–21 900	0–10·5
Cl^-/ppm	1·5	3·5–4·6
F^-/ppm	13	0·5–1·4
SO_2/ppm	0·4–2·0	0·9–1·0
SO_3/ppm	1·2–1·4	0·7–1·6

[*ppm by weight]

ture and gas flow rates remained constant, changes in the combustion air/gas ratio could lead to swings in condition from a high excess oxygen level to marginally oxidising. However, the residual oxygen, together with the oxygen partial pressure arising from the CO_2 and H_2O levels, would have been adequate to ensure stability of the SiO_2 in the oxide film and suppress loss as silicon monoxide (SiO) vapour.

SEM X-ray microspectroscopy (XMS) analyses of flue dust particles showed them to contain predominantly K, Cl, Si, Al and Ca, with lesser amounts of Na, Zn, S, Mn, Ti, Cr, and Fe. Between 70 and 95% of the particles were water soluble, and were mainly the fluorides and chlorides of K, Na, Al, and Ca; there were insoluble silicates of Al and Fe.

The surfaces of the corroded silicon nitride bars were covered with thick deposits of severely blistered material, most probably the result of nitrogen evolution from the underlying silicon nitride. The blisters appeared to consist of a glassy material, which had been liquid at the corrosion temperature, and one or more crystalline phases. XMS elemental analysis of material obtained from the blisters showed that they contained K, Si, Ca, Al, and Cl, and lesser amounts of Zn, S, and either Y, or Fe and Mg, depending on the base silicon nitride composition (Y for SN1, Fe and Mg for SN2). It appeared that the glasses were predominantly a potassium aluminosilicate, and that the crystals, on the bases of XMS analyses, were either a calcium yttrium silicate (SN1), or calcium magnesium silicate (SN2), together with the potassium aluminosilicate, $KAlSiO_4$: strong peaks for sodium potassium sulphate were identified by XRD.

3.2 Corroded SN1

XRD examination showed that the SN1, yttrium oxide-densified, silicon nitride contained β-silicon nitride as the major crystalline phase together with the intergranular yttrium-containing phases, SiY, $Y_2Si_3O_3N_4$ and $YNSiO_2$. A general microstructural

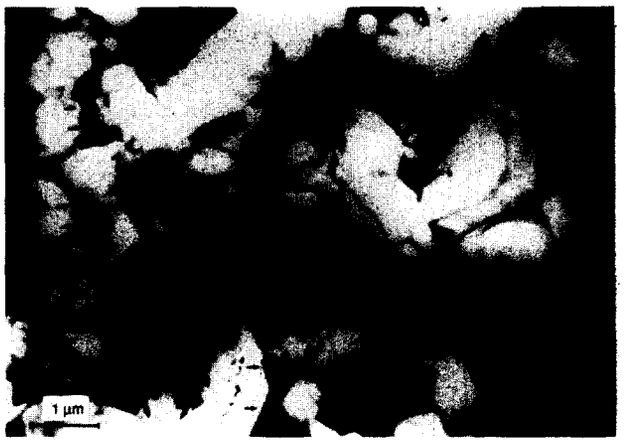

Fig. 1. A general planar view of corroded SN1 silicon nitride at the corrosion layer interface: light regions β-Si_3N_4 grains; the arrowed dark regions Y-rich phases which also contain Fe.

overview of uncorroded SN1 silicon nitride at the corrosion layer interface with unattacked material, and in a plane parallel to the external exposed surface, is provided by the TEM micrograph in Fig. 1. The light regions are β-silicon nitride grains; pockets of a yttrium-rich intergranular phase, which also contained Fe, are shown clearly as the dark regions (arrowed) at higher magnification coupled with XMS analysis (Fig. 2). Many of the yttrium-rich regions appeared to be interconnected. These micrographs are not distinguishable form those of uncorroded material. Figs 3 and 4 show planar sections, but now just within the corroded zone. Figure 3 illustrates the changes taking place in the intergranular region, with the appearance of 100–200 nm dimension regions of foamed glass (liquid at high temperature) at points where the (lighter) silicon nitride grains come into contact with wetting liquids. Because this figure shows a planar section at the corrosion front there is the likelihood that some of the grain boundaries seen are those of uncorroded material. There is here, however, an indication of penetration of a liquid-forming phase at the silicon nitride grain

Fig. 2. Corroded SN1 at high magnification: XMS analysis of dark regions showing the presence of Y and Fe.

Fig. 3. Corroded SN1: 100 to 200 nm regions of foamed intergranular glass at a Si_3N_4 grain, and (smaller arrows) indications of general intergranular attack.

boundary (both features arrowed). At higher magnification (Fig. 4(a)) ~10 nm dimension microvoid formation at a silicon nitride–silicon nitride grain boundary can be seen, leading in extreme cases to the complete grain face separation in Fig. 4(b). On the basis of the lighter colour of the void regions of Fig. 4(b) it is believed that they do not contain glass: whether the nm dimension, more spherical, regions of Fig. 4(a) are voids or glass microspheres is not so certain, but it is assumed that they are again gas-filled bubbles. The very fine scale of all these regions made reliable XMS analyses impossible.

3.3 Corroded SN2

The more heavily iron-contaminated and glassy SN2 silicon nitride also contained predominantly β-Si_3N_4, together with intergranular FeSi, $FeSi_2$, Si_2N_2O, and the Olivine $(Mg,Fe)SiO_4$ forsterite structure solid solution; glass was present at many three grain junctions, and identification of the Mg-containing secondary phase was assisted by XMS analysis. Figs 5(a) and (b) show typical regions of material at the corrosion zone interface after corrosion for 800 h. The MgO-containing silicon nitride was more severely degraded during corrosion than the SN1, Y_2O_3-densified silicon nitride. A marked feature of the microstructure of this material (arrowed) is the regions which appear to be completely depleted of glass, bounded by silicon nitride grains. These are not seen in uncorroded material and suggest the large-scale loss of a liquid (of lowered viscosity) from these regions. Figure 6 shows (arrowed) a crystalline

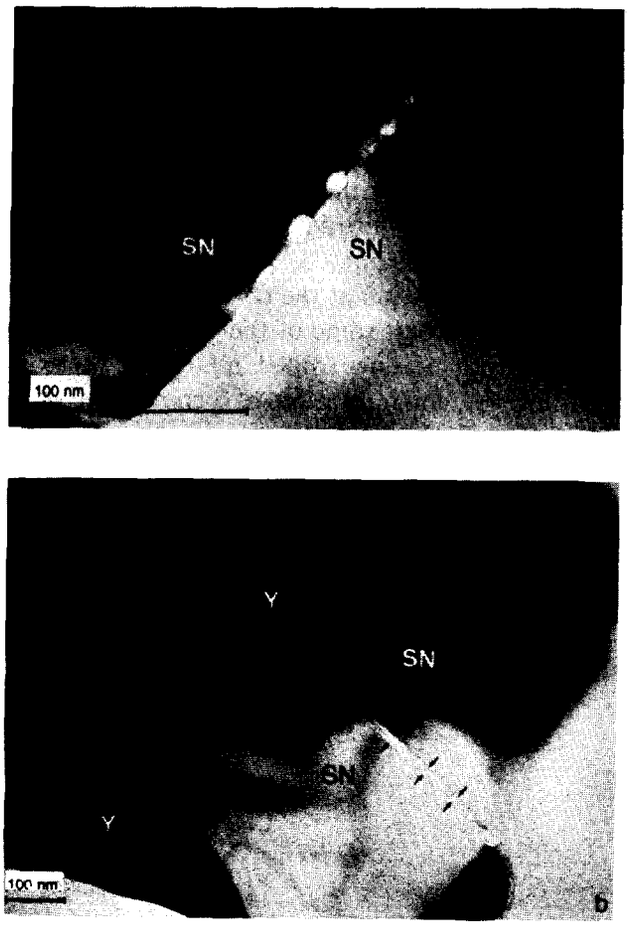

Fig. 4. (a) Nano-void formation at a silicon nitride-silicon nitride grain boundary; (b) complete grain face separation.

Fig. 5. Corroded SN2: typical planar view regions at the corrosion zone interface after corrosion for 800 h; arrows indicate intergranular voids foreign to the uncorroded microstructure.

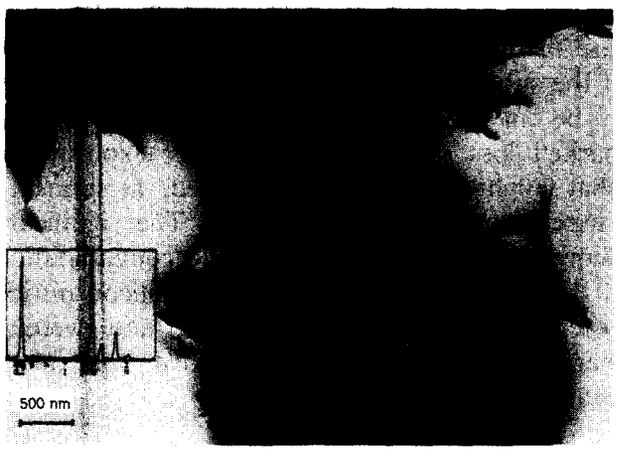

Fig. 6. Corroded SN2 at higher magnification: Fe-rich inclusions and evidence of extensive Zn contamination.

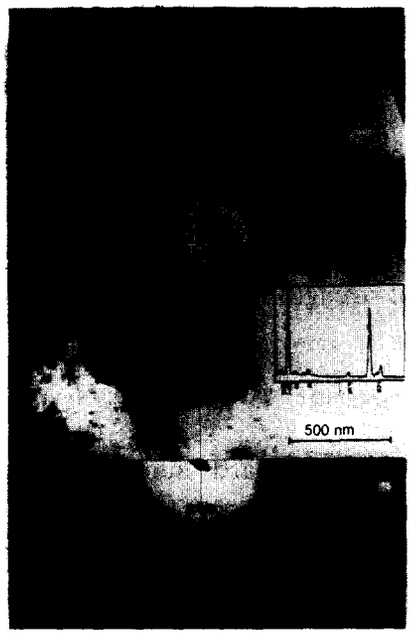

Fig. 7. Corroded SN2: proximity to the corroded external surface; arrowed phase identified by selected area diffraction as β-cristobalite.

Fe-rich intergranular phase, together with the corresponding XMS spectrum, suggesting that it is an iron silicide inclusion, which from the contacting angle with the bounding silicon nitride grains appears to be non-wetting. There is evidence from the XMS spectrum of significant penetration of flue gas Zn into this region of the material. This photograph also shows small neighbouring regions which appear to be devoid of glass.

Figure 7 shows a section of material nearer still to the surface. The arrowed phase was identified by SAD as predominantly β-cristobalite although some reflections could not be indexed. What may be relics of hexagonal symmetry silicon nitride grains are visible in the vicinity, and the appreciable amounts of S present in this film, in association with K and Zn, suggest the presence of sulphates.

Table 3. Strength and residual strength, after exposure at ~1050°C for 100 h

	4-point bend strength/MPa		
Material	*Uncorroded*	*Corroded*	*% loss*
SN1	610 ± 39 [20]	437 ± 62 [8]	28
SN2	610 ± 54 [10]	282 ± 38 [8]	54

3.4 Strength measurements

Bars of both materials, uncorroded and after corrosion for 100 h, were cut from the plates and broken in 4-point bend. The mean strengths and standard deviations, and the numbers of bars used for each series, are shown in Table 3. While both materials lost strength, the more glassy, magnesium oxide densified SN2 material was the most strongly affected by corrosion.

4 Discussion

These examinations using TEM showing details of the silicon nitride oxidative corrosion process under real industrial conditions, and the nature of some of the sub-surface events, indicate the usefulness of this technique for analysis of aspects of the high temperature corrosion of multiphase silicon nitride ceramics. A number of features of interest are revealed, the interpretation of which requires at this stage some speculation. The views put forward in this report are therefore regarded as tentative, but it is hoped that they will stimulate continued and more detailed examination of this type of reaction interface, and lead to a more complete identification of the complex processes occurring.

Analyses of the outer corrosion layer show that the surface at temperatures in the region of 1050°C was predominantly a low viscosity liquid potassium aluminosilicate. The susceptibility of the intergranular glass to reaction with corrodent metal oxide such as Al_2O_3 and K_2O is marked. This effect is seen most strongly with the glassy, MgO-densified, silicon nitride, although there is also very clear evidence for sub-surface attack in the more crystalline material hot-pressed with Y_2O_3 addition. Of significance is the evidence for the inwards diffusion of impurity cations into the intergranular phase of the silicon nitride, where they alter markedly the chemical and physical characteristics of the glass, and in particular its permeability towards oxygen.

The localised, uniform 10–15 nm dimension intergranular spherical features shown in Fig. 4(a) seem most probably to be nitrogen-filled bubbles generated by oxidation of the silicon nitride by

oxygen diffusing through an intergranular film. At this bubble dimension, and assuming a liquid–gas interfacial energy of ~300 mJ m^{-2}, the equilibrium internal gas pressure would be of the order of 600 bar. This is high, but is still insignificant by comparison with the theoretical nitrogen pressure in equilibrium with silicon dioxide and oxygen at 0·2 bar pressure at this temperature, which, on the basis of a standard Gibbs function of reaction at 1400 K of ~–1703 kJ mol^{-1}, would theoretically be of the order of 10^{30} bar. This pressure is clearly an unrealistic one from any practical point of view; the value is of interest in that it serves to indicate the marked tendency for nitrogen to be generated in these regions, and for it to be able to build up a considerable pressures. The internal gas pressure might then be able, in effect, to prise grains apart. This interpretation is, however, clouded by the possibility that internal stresses will be generated also by the considerable volume expansion (~86%) caused by oxidation of silicon nitride to SiO_2, and these stresses will add to those caused by nitrogen generation. The larger voids seen in Fig. 4(b) suggest that with time individual bubbles have indeed linked to form continuous cavities, from which liquid silicate has been expelled by the continuing generation of nitrogen. In the case of the more glassy SN2 material, giving on corrosion much larger liquid-free regions, the process appears to have occurred more extensively. That liquid mobility on this scale should occur at the relatively low temperature of 1100°C would require a very low viscosity, but this would be readily attained by the incorporation of K_2O into the intergranular phase.

Thus, the overall action of the liquid phase assisted corrosion process in generating the intergrain cavities is postulated to be a combination of enhanced oxygen permeation and therefore internal oxidation, and a lowered silicate liquid viscosity associated with K_2O enrichment. That the effect seems to be more marked in the case of the MgO-containing silicon nitride would be explicable partly in terms of a stronger effect of the Mg^{2+} ions on the liquid viscosity, by comparison with the trivalent Y^{3+}, but also because (on the basis of the XRD data) only part of the Y is incorporated into the intergranular glass. Evidence for the greater susceptibility of the MgO-densified silicon nitride to corrosion is provided also by the greater loss of strength of this material after exposure to the flue gas.

It may be speculated therefore that one of the important consequences of the intergranular oxidation of silicon nitride, as shown by this series of TEM photographs, is the loss of bonding of individual silicon nitride grains in the sub-scale region, and thus their incipient detachment. In the case of fully densified materials this deterioration of the sub-surface microstructural quality is likely to be an important factor responsible for the marked loss of strength seen after exposure to what might otherwise be regarded, in terms of temperature, as mild conditions. The significant changes during exposure to oxide contamination of the intergranular liquid in these silicon nitride systems, in composition, fluidity, and wetting characteristics, thus merit extended, and more detailed investigation.

5 Conclusions

Penetration of the intergranular phase of silicon nitride materials by the more mobile cations of a corrodent surface film leads to significant compositional changes in the subsurface intergranular liquid phase, to the development of nm dimension voids within the intergranular phase, and ultimately to local complete loss of contact between adjacent silicon nitride grains. This is postulated to be an important factor leading to the loss of mechanical strength in corroded materials.

Acknowledgement

This work has been partly supported by the Commission of the European Communities through Stimulation Action Contract ST2J-0146-UK(CD).

References

1. Luyten, J. & Stalios, A., In situ corrosion of SiC and Si_3N_4 in the flue gases of an Al-remelting furnace. *Werkstoffe und Korrosion*, **41** (1990) 734–5.
2. Luyten, J., Lemaitre, P. & Stalios, A., High temperature corrosion of silicon nitride and silicon carbide exposed to the flue gases of an aluminium remelting furnace. In *Proc. Eur. Colloquium, High Temperature Corrosion of Technical Ceramics*, ed. R. J. Fordham, Elsevier Applied Science, London 1990, pp. 161–5.
3. Stalios, A., Neyens, L. & Luten, J., In situ corrosion of silicon nitride and silicon carbide ceramics. In *Deutsche Keramische Ges. Symp. Proc. Verschliess und Korrosion–Keramic in der Anwendung*, 22–23 May 1990, pp. 244–50.
4. Mayer, M. I., & Riley, F. L., Sodium assisted oxidation of reaction bonded silicon nitride. *J. Mat. Sci.*, **13** (1978) 1319–28.
5. Mayer, M. I. & Riley, F. L., Sodium ion assisted oxidation of reaction bonded silicon nitride. In *Proc. Brit. Ceram. Soc.*, No. 26, July 1978, pp. 251–64.
6. Fox, D. S. & Jacobson, N. S., Molten salt corrosion of silicon nitride: I. sodium carbonate. *J. Amer. Ceram. Soc.*, **72**(2), (1988) 128–38.
7. Gauthier, G., Lamkin, M. A., Riley, F. L. & Fordham, R. J., High temperature liquid corrosion of silicon nitride based materials. In *Ceramics in Energy Applications*, Pro-

ceedings of the Institute of Energy Conference, Sheffield 9–11 April 1990, Adam Hilger, Bristol 1990, pp. 49–58.
8. Lamkin, M. A., Riley, F. L. & Fordham, R. J., Hot corrosion of silicon nitride in the presence of sodium and vanadium compounds. In *Proc. Eur. Colloquium, High Temperature Corrosion of Technical Ceramics*, ed. R. J. Fordham, Elsevier Applied Science, London 1990, pp. 53–68.
9. Riley, F. L., Phase equilibrium relationships and the liquid phase assisted oxidative corrosion of silicon nitride. In *Corrosion of Advanced Ceramics; Measurement and Modelling*. NATO ASI Series E: Applied Sciences — Vol. 267. ed. K. G. Nickel, Kluwer Academic Publishers. Dordrecht, 1994 pp. 85–96.
10. Lamkin, M. A., Riley, F. L. & Fordham, R. J., Oxygen mobility in silicon dioxide and silicate glasses: a review. *J. European Cer. Soc.*, **10**(5) (1992) 347–67.
11. Andrews, P. & Riley, F. L., The microstructure and composition of oxide films formed during high temperature oxidation of sintered silicon nitride. *J. European Cer. Soc.*, **5**(4) (1990) 245–56.
12. Urbain, F., Cambier, F., Deletter & Anseau, M., Viscosity of silicate melts. *T. & J. Brit. Ceram. Soc.*, **80**(4) (1981) 139–41.
13. Popper, P., Sintering of silicon nitride: a review. In *Progress in Nitrogen Ceramics*, ed. F. L. Riley, Martinus Nijhoff, The Hague, 1983 pp. 187–210.
14. Stalios, A. D., Luyten, J., Hemsley, C. D., Riley, F. L. & Fordham, R. J., The interaction of iron during the hot-pressing of silicon nitride. *J. European Ceram. Soc.*, **7** (1991) 75–81.
15. Kleebe, H. -J., High-resolution electron microscopy studies on Si_3N_4 ceramics. In *Silicon Nitride 93*, Key Engineering Materials Vol. 89–91, Trans Tech Publications, Switzerland 1994 pp. 339–44.